Structural and Functional Characterisation of Multi-copper Oxidase CueO from Lignin-Degrading Bacterium *Ochrobactrum* sp. Reveal its Activity towards Lignin Model Compounds and Lignosulfonate

Rommel Santiago Granja-Travez[1], Rachael C. Wilkinson[2], Gabriela Felix Persinoti[3], Fabio M. Squina[3], Vilmos Fülöp[2], and Timothy D.H. Bugg[1]*

1. Department of Chemistry, University of Warwick, Coventry CV4 7AL, UK
2. School of Life Sciences, University of Warwick, Coventry CV4 7AL, UK
3. Programa de Processos Tecnológicos e Ambientais, Universidade de Sorocaba, Sorocaba, Brazil

Corresponding author: Prof. Timothy D.H. Bugg, Department of Chemistry, University of Warwick, Coventry CV4 7AL, United Kingdom. Email T.D.Bugg@warwick.ac.uk, tel 44-2476-573018.

Running title: Multi-copper oxidase CueO from *Ochrobactrum* sp.

Keywords: Multi-copper oxidase; laccase; Ochrobactrum; lignin oxidation.

Database: structural data are available in the PDB under the accession number 6EVG

Abstract:

The identification of enzymes responsible for oxidation of lignin in lignin-degrading bacteria is of interest for biotechnological valorization of lignin to renewable chemical products. The genome sequences of two lignin-degrading bacteria, *Ochrobactrum* sp., and *Paenibacillus* sp., contain no B-type DyP peroxidases implicated in lignin degradation in other bacteria, but contain putative multi-copper oxidase genes. Multi-copper oxidase CueO from *Ochrobactrum* sp. was expressed and reconstituted as a recombinant laccase-like enzyme, and kinetically characterized. *Ochrobactrum* CueO shows activity for oxidation of β-aryl ether and biphenyl lignin dimer model compounds, generating oxidized dimeric products, and shows activity for oxidation of Ca-lignosulfonate, generating vanillic acid as a low molecular weight product. The crystal structure of *Ochrobactrum* CueO (OcCueO) has been determined at 1.1 Å resolution (PDB: 6EVG), showing a four-coordinate mononuclear type I copper centre with ligands His495, His434 and Cys490 with Met500 as an axial ligand, similar to that of *E. coli* CueO and bacterial azurin proteins, whereas fungal laccase enzymes contain a three-coordinate type I copper metal centre. A trinuclear type 2/3 copper cluster was modelled into the active site, showing similar structure to *E. coli* CueO and fungal laccases, and three solvent channels leading to the active site. Site-directed mutagenesis was carried out on amino acid residues found in the solvent channels, indicating the importance for residues Asp102, Gly103, Arg221, Arg223 and Asp462 for catalytic activity. The work identifies a new bacterial multi-copper enzyme with activity for lignin oxidation, and implicates a role for bacterial laccase-like multi-copper oxidases in some lignin-degrading bacteria.

Abbreviations: ABTS, 2,2'-azino-bis(3-ethylthiazoline-6-sulfonate; SGZ, syringaldazine; DCP, 2,4-dichlorophenol; DMP, 2,6-dimethoxyphenol; GGE, guaiacylglycerol-β-guaiacyl; DDVA, 2,2'-dihydroxy-3,3'-dimethoxy-5,5'-dicarboxybiphenyl

Introduction

The aromatic heteropolymer lignin constitutes 15-30% of the lignocellulose cell wall in plant biomass, and represents an abundant renewable raw material for conversion via either biocatalysis or chemocatalysis into aromatic chemicals. The microbial oxidation of lignin has been studied extensively in white-rot fungi, which produce extracellular lignin peroxidase and laccase enzymes for lignin oxidation [1, 2], but recently bacterial enzymes for lignin oxidation have also been discovered in some soil bacteria [3, 4]. Dye decolorizing peroxidases DypB in *Rhodococcus jostii* RHA1 [5], Dyp2 in *Amycolatopsis sp.* 75iv2 [6] and Dyp1B in *Pseudomonas fluorescens* [7] have been shown to be active for oxidation of polymeric lignin and lignin model compounds, and Lin et al have reported that a B-type dyp gene in *P. putida* A514 is overexpressed 68-fold in the presence of alkali Kraft lignin [8]. On the other hand, laccases are a group of enzymes that can oxidise a huge range of substrates without any additional cofactor, producing water as the only byproduct [9], making them a group of enzymes with a huge potential for scientific and industrial applications.

Although the precise role of laccase enzymes in lignin degradation is uncertain [10, 11], deletion of the *Streptomyces* laccase gene has been shown to lead to reduced amounts of acid-precipitable lignin (APPL) formation from lignocellulose, implying a role for this laccase in lignin oxidation [12]. The biological function of bacterial laccases are thought to include morphogenesis [13], biosynthesis of a spore pigment for UV and hydrogen peroxide protection [14], and copper homeostasis [15, 16]. Several factors suggest that their biological function is diverse and may vary from one organism to another, namely: the wide range of laccase substrates; low sequence homology in the laccase protein family; the presence of different types of laccases including 2- and 3-domain laccases, with and without signal peptides for protein exportation; and the existence of putative laccases in anaerobic bacteria [17]. Bacterial laccase-like multi-copper oxidases have been reported in *Bacillus subtilis* [18], *Bacillus pumilus* [19], *Bacillus clausii* [20], *Bacillus licheniformis* [21], *Streptomyces coelicolor* [22], *Streptomyces sviceus* [23], *Meiothermus ruber* [24], *E. coli* [25], and in *Bacillus coagulans*, *Gramella forsetti*, *Streptomyces pristinaespiralis*, *Marivirga tractuosa*, and *Spirosoma linguale* [26]. In general, bacterial laccases tend to be more thermostable and resistant to hard alkali pH or salinity conditions than their fungal counterparts [18-20, 24], and their expression on *E. coli* is easier and gives relatively high yields, although it usually requires oxygen-limited growth conditions to obtain fully copper loaded proteins [26, 27].

Currently only a small number of bacteria with the ability to oxidise lignin have been studied in detail: lignin-oxidising enzymes have been characterized in *Rhodococcus*, *Amycolatopsis*, *Pseudomonas* and *Streptomyces* [5-7, 12]; and transcriptomic studies have been reported in *Pseudomonas putida* A514 [8]. We have reported the isolation of soil bacteria with lignin oxidation capability from woodland soil and from municipal waste soil [28, 29]. We have therefore investigated via genome sequencing and protein characterization whether these organisms use similar strategies for lignin oxidation. Here we report the identification of a novel bacterial laccase-like multi-copper oxidase from lignin-degrading *Ochrobactrum* sp..

Results

Identification of genomic sequences encoding multicopper oxidase enzymes in Ochrobactrum sp. and Paenibacillus sp.

The genome sequences of *Ochrobactrum* sp. and *Paenibacillus sp.* were examined for the presence of genes encoding potential lignin oxidation enzymes, and aromatic degradation pathways that could metabolize the low molecular weight products of lignin breakdown. However, the *Ochrobactrum* sp. genome contained only one A-type dyp gene (gene ID 4966), and the genome of *Paenibacillus* sp. contained no dyp-type genes. Previous literature studies in *Rhodococcus jostii* [5] and *Pseudomonas fluorescens* [7] have indicated that activity for lignin oxidation is found in B-type DyP peroxidases, but not A-type DyP peroxidases.

The genome of *Ochrobactrum* sp. contains a multi-copper oxidase gene *cueO* (gene ID 4352, with 91.4% sequence identity to Uniprot E2GIP7_9RHIZ), immediately adjacent to a *sodC* gene encoding a Cu/Zn superoxide dismutase gene. The genome of *Paenibacillus* contains a putative polyphenol oxidase YlmD (gene ID 6155, with 41.4% sequence identity to Uniprot YLMD_BACSU), predicted by a BLAST analysis in Uniprot (http://www.uniprot.org/). These two genes were therefore selected for protein expression, as described above. Extracellular manganese superoxide dismutase SodA from *Sphingobacterium* sp. T2 has recently been shown to have activity for lignin oxidation [30]. The *Ochrobactrum* sp genome contains three superoxide dismutase genes, two *sodF* genes (ID 773, 4095) and the *sodC* gene (ID 4353) noted above, but none of these genes contained a signal sequence for protein export. The *Paenibacillus* genome contained two superoxide dismutase genes, a *sodM* gene (ID 6086) and a *sodF* gene (ID 6093), but neither gene contained a signal sequence for protein export.

The metabolism of lignin degradation products via bacterial aromatic degradation pathways is supported by several pieces of evidence: the accumulation of vanillic acid as a metabolite in lignin degradation, and the generation of vanillin as a bioproduct of

lignocellulose breakdown in a *vdh* gene deletion mutant of *Rhodococcus jostii* RHA1 [31]; the generation of pyridine-dicarboxylic acids from re-routing of lignocellulose breakdown in *R. jostii* [32]; and the overexpression of genes on the β-ketoadipate pathway of *P. putida* A514 in the presence of lignin [8]. The genome of *Ochrobactrum* sp. contains a gene cluster at 4452-4463 encoding the β-ketoadipate pathway, and also contains five of the genes on the 4-hydroxyphenylacetate pathway (at 96, 97, 104, 105, 1962 and 1964), and *mhqDE* genes (at 2570-71) for hydroquinone utilization. In contrast, the *Paenibacillus* sp. genome does not contain the central β-ketoadipate gene cluster, although there are genes for hydroquinone utilization: a *mhqDOPR* cluster at 2217-2220, and *mhqA* genes at 3761 and 4617.

Protein expression & purification

The genes encoding *Ochrobactrum* CueO and *Paenibacillus* polyphenol oxidase (P-PPO) were amplified from chromosomal DNA, and cloned into expression vector pET151. The recombinant proteins were then expressed as N-terminal His6 fusion proteins in E. coli, after induction with 1 mM IPTG, grown in Luria Bertani media supplemented with 80 μM $CuSO_4$. The recombinant proteins were purified by immobilized metal ion chromatography (IMAC), which gave the expected protein bands at 55.1 kDa for OcCueO and 33.4 kDa for P-PPO (see Figure 1A). The His_6 fusion tag was then removed by proteolytic digestion with TEV protease, followed by further purification by a second IMAC, to give recombinant proteins free of impurities. Yields of ≈20 mg OcCueO and ≈60 mg P-PPO per litre of culture were obtained.

Expression of recombinant CueO in *E. coli* BL21 was found to be dependent on the conditions used for protein expression. Under aerated incubation achieved by shaking, the purified protein was found to be dependent upon exogenous Cu^{2+} salts for activity and it was colorless in solution; but using the conditions reported by Durao [27] involving microaerobic conditions, achieved by switching off the shaking function during incubation after IPTG induction, the enzyme was active without exogeneous copper and was blue in colour, showing a typical UV/vis spectrum for laccase enzymes (λ_{max} 612 nm , see Figure 1B), at a protein yield of 7 mg per liter of bacterial culture. The purified enzyme was analysed by inductively coupled plasma optical emission spectroscopy (ICP-OES), giving a stoichiometry of 4.8 ± 0.8 mol Cu per mol protein.

Kinetic characterization of OcCueO and P-PPO

Recombinant OcCueO and P-PPO were assayed for activity with 2,2'-azino-bis(3-ethylthiazoline-6-sulfonate (ABTS); syringaldazine (SGZ); 2,4-dichlorophenol (DCP); 2,6-

dimethoxyphenol (DMP) and guaiacol. P-PPO showed no activity using these substrates, but OcCueO was active with all substrates, and for the holoenzyme expressed and purified as described above, activity did not require addition of exogenous Cu^{2+} ions. Addition of hydrogen peroxide gave no effect on enzyme activity, hence OcCueO shows only oxidase activity, not peroxidase activity. Steady state kinetic parameters were measured for OcCueO using ABTS, SGZ, and DMP as substrates. The enzymes showed similar k_{cat} values of 0.46-0.93 s^{-1} for the three substrates, but a lower K_M of 4 μM for SGZ, giving a k_{cat}/K_M value of 1.1 x 10^5 M^{-1} s^{-1} for this substrate (see Table 1). The pH-rate profile of OcCueO was measured using ABTS and SGZ as substrates. As illustrated in Figure 2A, using ABTS the optimum pH range was 3.0-5.0, with maximum activity at 4.0; while using SGZ the optimum pH range was 6.5-9.0, with maximum activity at pH 7.6-8.6.

The activity of OcCueO was compared against commercially available fungal *Trametes versicolor* laccase (TvL). The specific activity of OcCueO towards ABTS was 30-fold less than TvL. However, the specific activity of OcCueO towards SGZ was 40-fold higher than TvL (see Figure 2B), implying that OcCueO may show a better activity and potential for certain applications.

Protein stability of bacterial laccase OcCueO vs fungal laccase TvL at 50 °C was assessed, using ABTS as substrate. Results showed that after an initial loss of 40% activity after 30 min, OcCueO retained the residual catalytic activity over a further 6 hours, whereas TvL showed only 20% residual activity after this time (see Figure 2C), indicating that OcCueO is more thermostable than the commercial laccase TvL.

Activity of Ochrobactrum CueO against lignin model compounds and polymeric lignin substrates

In order to study whether OcCueO could oxidise lignin substrates, recombinant OcCueO was first assayed against two lignin model compounds: β-aryl ether dimer guaiacylglycerol-β-guaiacyl (GGE); and biphenyl dimer 2,2'-dihydroxy-3,3'-dimethoxy-5,5'-dicarboxybiphenyl (DDVA), with and without the addition of 1 mM ABTS as mediator, and products monitored by HPLC. OcCueO was active regardless the presence of a mediator, though the presence of a mediator resulted in variations in some chromatogram peaks. As shown in Figure 3A, incubation of OcCueO with GGE gave a visible colour change in solution, and led to the appearance of three new product peaks by HPLC analysis. Analysis of these peaks by electrospray mass spectrometry showed that major product peaks P1 and P2 contained higher molecular weight compounds at *m/z* 573.28 and 695.32 respectively (compared with 343.28 Da for GGE), while the smaller peak P3 gave *m/z* 303.2. Peaks P1 and P2 therefore

appear to correspond to oxidative dimerization products of GGE. The peak P3 appeared only when the reaction was carried out in absence of the mediator.

Incubation of OcCueO with DDVA also gave a visible colour change in solution, and the appearance of four new product peaks by HPLC analysis. Analysis of these peaks by electrospray mass spectrometry gave *m/z* 687 for peak P1, which appeared only in presence of the mediator; while peaks *m/z* 621, 605 and 663 for P2, P3 and P4, respectively, were obtained only in absence of the mediator (see Figure 3B). All peaks showed higher molecular weight compounds (compared with 335 Da for DDVA), indicating that OcCueO also catalyzed an oxidative dimerization reaction upon DDVA, followed by further modification reactions. Assignment of structures for these peaks and possible mechanisms for their formation will be discussed in the Discussion section.

Recombinant OcCueO was then incubated with eight different lignin preparations, including organosolv lignins, alkali lignins, lignosulfonate, and industrial Kraft lignin, in presence and absence of mediators (ABTS and SGZ were used as mediators). Colour changes were observed in each case, indicating a reaction with polymeric lignin, however only in one case a low molecular weight product was detected by HPLC analysis. As shown in Figure 3C, in the case of Ca-lignosulfonate, a new peak was formed at 27 min retention time, whose retention time and mass spectrum matches with that of vanillic acid (*m/z* 169 MH^+, 191 MNa^+). The presence of ABTS as mediator slightly increased the size of this peak.

Crystal Structure of OcCueO

The crystal structure of OcCueO has been determined at 1.1 Å resolution (PDB accession 6EVG). The asymmetric unit of the crystal contained one molecule with the space group $P2_1$. The structure shows OcCueO to be a monomer organised into three separate domains (see Figure 4), as is typically observed for multicopper binding proteins [25, 33, 34]. The domains of OcCueO are divided as follows; domain one (residues 22-160), domain two (residues 161-318) and domain three (residues 319-507). Each of the three domains shares similarities to the β-barrel type architecture observed in azurin and plastocyanin [35].

Structure of Mononuclear Copper Centre

The mononuclear (T1) copper centre within domain 3 of the OcCueO structure contains a four-coordinate trigonal pyramidal copper ion ligated by His495, His434 and Cys490 with Met500 as an axial ligand (see Figure 5A). This co-ordination is the same as that observed in azurin [36] and other bacterial laccases such as *E. coli* CueO [25] (see Figure 5B). Conversely,

the structure of *T. versicolor* laccase (PDB: 1GYC) also shown to have activity for lignin oxidation, demonstrates a trigonal coplanar co-ordination of the T1 copper (see Figure 5C) which is more typically seen amongst fungal laccases [33, 34]. Within fungal laccases the methionine residue is replaced with either a phenylalanine [33] or leucine [34] residue which is unable to act as an axial ligand for the copper ion.

It was not possible to trace residues 350-391 in the OcCueO structure, but a similar observation was reported for the *E. coli* CueO crystal structure, in which residues 380-403 could not be modelled [25]. In EcCueO, these residues pertain to an additional α-helix which lies near the T1 copper centre [25]. Within the OcCueO structure these residues also appear to be positioned in front of the T1 copper site. The presence of an additional α-helical loop covering the T1 copper centre reduces the size of the substrate binding pocket and has currently only been observed in bacterial laccases. This reduced substrate binding pocket could perhaps explain the preference for SGZ over ABTS.

Structure of Trinuclear Copper Centre

Within the OcCueO trinuclear (T2/3) copper centre no clear electron density was observed for the three copper ions (see Figure 6A). The difficulty to model laccases with a full complement of copper ions has previously been noted in the literature [25, 37]. The possibility of X-ray induced radiation damage [38,39] was considered as a possible explanation for the lack of copper ion electron density, however, careful analysis of the OcCueO dataset using wedges of data showed no electron density for the T2 and T3 copper ions from the first wedge of data onwards, therefore it seems most likely that copper ions were missing from the crystals, which were grown aerobically.

The copper ions at this site are typically co-ordinated by a group of eight highly conserved histidine residues [33, 34]. All the conserved histidines can be clearly assigned in the OcCueO structure (see Figure 6A). Copper ions were modelled into the OcCueO structure using co-ordinates from the structurally similar *E. coli* CueO structure (PDB: 3NSF) to confirm the positioning of the T2/3 site (see Figure 6B). The T2/3 copper site is embedded between domains one and three of OcCueO with both domains containing residues putatively involved in copper co-ordination. Superposition of the apo-OcCueO T2/3 site with that from the fully occupied *E. coli* CueO (PDB: 4E9Q [40]) shows that both His131 and His93 are in a significantly different conformation (see Figure 6C). This alteration is suggestive of these two histidines having a key role in the co-ordination of the type II copper. Minor alterations in conformation can also be seen for His133, His439 and His91. The positions of both His491

and His489 are, however, almost identical to their *E. coli* CueO counterparts. A ModBase [41] model calculated using the sequence for OcCueO generates a T2/3 site near identical in conformation to that observed for the fully occupied *E. coli* CueO (PDB: 4E9Q) site.

Solvent channels

Three putative solvent channels leading to the T2/3 copper site within OcCueO structure were identified using CAVER 3.0 [42] (see Figure 7, residues listed in Table 2). Two of the channels originate from the modelled T3 copper ions and are situated between domains one and two (see Figure 7A). Each of these channels has only one mapped solvent access point but a shared entry at the T2/3 copper site. A further putative solvent channel originating from the modelled T2 copper ion was identified (see Figure 7B). This differs slightly from the solvent channels mapped in *M. albomyces* [43] and *L. tigrinus* [44] laccases where only two channels are described, one accessing the T2 copper side of the trinuclear centre and the other channel accesses the T3 copper side. Solvent channels originating from the T2/3 site are important in facilitating access of the site to oxygen and in the subsequent release of water molecules formed during the reaction [44].

Site directed mutagenesis

The functional differences between bacterial and fungal laccases are not yet well understood, and few literature studies have been published on this topic. Laccase amino acid sequences typically contain well conserved amino acid motifs that are involved in copper binding: HXHG, HXH, HXXHXH and HCHXXXHXXXXM/L/F, and these sequence motifs are present in both fungal and bacterial laccases [17, 26, 45]. Bacterial laccases have been reported to show lower redox potentials than their fungal counterparts [46], hence they can oxidise a smaller range of substrates, but in contrast, they are usually easier to clone and express in *E. coli* with relatively high yields [26, 27], whereas fungal laccases with higher redox potential tend to be more difficult to clone and express [47-49].

To gain some insights into structural differences and similarities between bacterial and fungal laccases, a multiple sequence alignment was performed with 32 fungal laccases and 33 bacterial laccases or multicopper oxidases sequences. Two groups of amino acid residues were observed: Group 1 contained amino acid residues that are found in >90% of fungal and bacterial sequences, while group 2 contained amino acid residues near to copper centres that are conserved only in high redox potential laccases (HRPL) and apparently absent in bacterial

laccases (see Table 3). A partial amino acid sequence alignment, containing each of the residues mentioned in Table 5, is shown in Figure 8.

Some of the conserved Group 1 residues form part of the previously described channels, as shown in Figure 7, so therefore they might play a role in oxygen or water transportation to the trinuclear copper center. Residue Gly145 was found to be present in the 100% of the analyzed sequences and it is overlapping the two channels from the T3 copper ions (see Figure 7A); while residues Asp102, Asp249, Arg269 and Asp462 are present in the channel from the T2 copper side (see Figure 7B). Arg221 and Arg223 appear to form part of a continuation of this tunnel in the fungal laccase TvL (PDB 1GYC). Site-directed mutants 1 (K461A, D462A), 2 (R221A, R223A), and 3 (D102A, G103A) were generated in order to study the function of amino acids in these channels by replacement with alanine. Mutants 4 (S126G, F127T, N128F) and 8 (K461R) replaced amino acid residues in these solvent channels by residues commonly present in high redox potential laccases.

For Group 2, two regions were found with a high similarity among HRPL but with a no homology among bacterial laccases (see Table 5): residues Lys482, Ser483, His484 and Phe486 are found as NPGxW in fungal laccases; and residues Ile109, Ala110, Ala111 and Gly112 are found as QCPI in fungal laccases. Site-directed mutants 5 (I109Q, A110C, A111P), 6 (F486W, M487L) and 7 (K482N, S483P, H248G) were constructed in order to explore whether these amino acid replacements would lead to higher catalytic activity.

After cloning and protein expression, all mutant proteins were successfully purified, and assayed for activity with ABTS and SGZ as substrates, and the results are shown in Figure 9. Mutants 1 and 2 showed no observable activity, although they were expressed at lower levels than the wild-type protein. The lack of activity indicates the importance of residues Lys461, Asp462, in the solvent channel from the T2 copper side, and a significant role for residues Arg221 and Arg223, though the lower expression suggests the possibility of a local structural change. Mutant 8 (K461R) lost >80% catalytic activity, indicating a specific preference for lysine at position 461, and mutant 3 also lost >80% catalytic activity, indicating a significant role for Asp102/Gly103 in the solvent channel from the T2 copper. We note that some of the new highly conserved residues (Asp102, Arg221, Arg223, Asp249, Arg269 and Asp462) are forming part of the channel from the T2 copper, and part of this channel is located in domain 2, suggesting that this region may play an important role in laccase activity.

Discussion

In this paper we have identified and characterized a new bacterial multi-copper oxidase from *Ochrobactrum* sp. Although several bacterial multi-copper oxidases have been identified (see Introduction), the only other bacterial laccases shown to have activity for polymeric lignin or lignin model compounds are the *Streptomyces* small laccases [12]. The activity of *Ochrobactrum* sp. CueO towards polymeric lignin and lignin model compounds suggests a role in lignin oxidation, and hence that some bacteria may utilize multi-copper oxidases for lignin oxidation.

The oxidation products formed from oxidation of lignin model compounds are indicative of oxidative dimerization, which has been observed for oxidation of phenolic model compounds by fungal laccase enzymes [50]. The oxidation product P1 obtained from β-aryl ether lignin dimer GGE is consistent with molecular formula $C_{33}H_{33}O_9$ (observed *m/z* 573.28, calculated *m/z* 573.21), which could be formed by oxidative dimerization of GGE, followed by fragmentation of the β,γ-bond of one monomer, with loss of formaldehyde, followed by a dehydration reaction. The oxidation product P2 obtained from biphenyl lignin dimer DDVA is consistent with molecular formula $C_{31}H_{25}O_{14}$ (observed *m/z* 621.12, calculated *m/z* 621.12), which could be formed by oxidative dimerization of DDVA, followed by decarboxylation of one subunit, and a subsequent two-electron oxidation. The formation of vanillic acid as a product from lignosulfonate oxidation implies cleavage of the α,β-bond of lignin units, and oxidation of the α-carbon centre.

The involvement of *Ochrobactrum* CueO in lignin oxidation differs from the role of *E. coli* CueO in copper resistance [15, 16], however we note that in the *Ochrobactrum* genome, the *cueO* gene was not clustered with any copper resistance genes, hence it appears to have a different function in this organism. Despite an apparent functional similarity to laccases from white-rot fungi, there are several structural features of OcCueO that link it more closely to that of *E. coli* CueO. Notably, the presence of an axial methionine ligand for the T1 copper site and the presence of an alpha-helical loop in front of the T1 copper site are both similar to the EcCueO structure. Previous work by Durao *et al* showed that mutation of the axial methionine residue to Phe or Leu, typically found in fungal laccases increased the redox potential of *B. subtilis* CotA by about 100 mV [51]. The additional alpha-helical loop at the T1 site is not found in fungal laccases, but does not prevent the oxidation of polymeric lignin or lignin model compounds by OcCueO. Furthermore, there appear to be differences between the solvent channels originating from the T2/3 site within CueO and those reported for fungal

laccases [34,43] or EcCueO [25]. The structures of white rot fungal laccases have been recently reviewed by Orlikowska et al [52].

The enzymology of bacterial lignin oxidation is still emerging, but there does appear to be diversity in the genes responsible for bacterial lignin oxidation [53]: some bacteria such as *Rhodococcus jostii* and *Pseudomonas putida* appear to utilize DyP-type peroxidases for lignin oxidation, whereas other bacteria such as *Ochrobactrum* sp. utilize multi-copper oxidases. Diversity of lignin-oxidising genes is also observed in basidiomycete fungi: the genome of *Phanerochaete chrysosporium* contain many lignin peroxidase genes [54], whereas the genome of *Schizophyllum commune* contains no lignin peroxidase genes but two laccase genes [55]. For oxidation of such a complex substrate, the use of multiple catalytic strategies is perhaps not surprising, and may offer advantages in different ecological niches.

Materials and methods

Genomic DNA sequencing of Ochrobactrum sp. and Paenibacillus sp.

Ochrobactrum sp. and *Paenibacillus sp*. were isolated previously as lignin-degrading strains from woodland soil [28] and municipal waste soil [29]. Genomic DNA from *Ochrobactrum sp*. and *Paenibacillus sp*. strains, was extracted using FastDNA SPIN Kit for soil (MP Biomedicals, Irvine, CA) according to the manufacturer's instructions. DNA quality and integrity were assessed by electrophoresis in a 0.8 % agarose gel, and DNA concentration was measured by fluorimetry (Qubit® 2.0 Fluorometer-Life Technologies. Carlsbad, California, EUA). 30ng of total DNA for each strain was used for library construction using Nextera® DNA Library Preparation Kit (Illumina, San Diego, CA), according to the manufacturer's instructions, except for the fragmentation step, that was performed at 58^{o}C for 5 minutes. Nextera libraries were pooled in equimolar concentrations and sequenced on Illumina HiSeq 2500 system at CTBE NGS sequencing facility, generating 5,474,812 and 5,810,807 paired-end reads of 2x100 bp (insert size, 300 bp), for *Ochrobactrum* sp. and *Paenibacillus* sp. strains, respectively.

Paired-end reads were preprocessed with Trimmomatic [54], to remove adapter and low-quality sequences, resulting in 4,335,623 and 5,169,654 high-quality reads, respectively. The genome size of *Ochrobactrum* sp. was estimated to be 5.3 Mb, while the genome of *Paenibacillus* sp. 7,2 Mb, based on k-mer count statistics accessed with Kmergenie, with an estimated coverage of approximately 150X. Genome assembly was carried out with SPAdes v3.6.2 [55] using an ensemble of k-mer values (21, 33, 47, 55, 77). The presence of typical bacterial marker genes was assessed using Phyla-Amphora [56]. The resulting assembly for

Ochrobactrum sp. has 87 scaffolds, with a total length of 5,310,057 bp and an N50 of 150,153 bp. The average GC content of the genome is 56.2%. *Paenibacillus* sp. genome assembly has 40 scaffolds, with a total length of 7,187,707 bp and an N50 of 353,719 bp. The average GC content of the genome is 43.5%.

Gene prediction was carried out with GeneMark [57] and PROKKA Prokaryotic Genome Annotation Pipeline [58]. A total of 5,269 genes were identified in *Ochrobactrum* sp. genome, of these, there are 5,210 are protein-encoding genes, 3 rRNA genes, 54 tRNAs, and 1 tmRNA. Regarding 16S rRNA, *Ochrobactrum* sp. presents 98.99% sequence similarity with *Ochrobactrum pecoris* O8RB2639 (T) and 98.13% with *Ochrobactrum rhizosphaerae* PR17(T), analyzed through EZBioCloud webserver identity tool [59]. A total of 6475, genes were identified in *Paenibacillus* sp. genome, of these, there are 6,405 are protein-encoding genes, 1 rRNA gene, 68 tRNAs, and 1 tmRNA. Regarding 16S rRNA, *Paenibacillus* sp. presents 99.45% sequence similarity with *Paenibacillus etheri* SH7 (T) and 98.66% with *Paenibacillus odorifer* DSM 15391(T). Genes of relevance to lignin oxidation and aromatic degradation are listed in Supporting Information Table S1 for *Ochrobactrum sp*. and Table S2 for *Paenibacillus sp*.

Cloning of Ochrobactrum CueO (OcCueO) and Paenibacillus polyphenol oxidase domain (P-PPO)

Genomic DNA was isolated using a Wizard Genomic DNA Purification Kit (Promega). The designed primers were as follows: Forward (5' CACC CAG GAC GCT CAC CAG AAA ATG 3') and Reverse (5' CTA TAC TGT TAC GAA CTG AGC CAT C 3') for *OcCueO,* which allowed to exclude a predicted tat-signal peptide at the beginning of the nucleotide sequence, and Forward (5' CACC ATG GAA CCG TTT GTG CAG GGG AAG 3') and reverse (5' TCA ACT CTC CTT TAT TCC GAT CCA G 3') for *p-ppo* (no signal peptide was predicted for this gene). These genes were amplified from genomic DNA by polymerase chain reaction using Pfx Taq polymerase. The PCR products (1.5 kbp for *OcCueO* and 0.8 kbp for *pae-lac*) were excised from a 1% agarose gel, purified by GeneJET PCR Purification Kit (Thermo Scientific), cloned into a pET151/D-TOPO vector (Invitrogen), following manufacturer's protocol, and transformed into One Shot TOP10 competent cells (Invitrogen). After correct DNA sequence confirmation by DNA sequencing, the plasmids were extracted and transformed into One Shot BL21 competent cells (Invitrogen) for protein expression.

Expression and purification of recombinant enzymes

The same procedure was followed for OcCueO and P-PPO expression. As starter culture, a Luria-Bertani broth (LB) supplemented with ampicillin was inoculated with BL21 cells harbouring the corresponding plasmid for expression of OcCueO or P-PPO. 10 mL of starter culture were used to inoculate 1 L of culture medium consisting of 25 g of LB media and 150 µg of ampicillin. The culture was grown at 37 °C for 3 to 5 h until it reached $A_{595} \approx 0.6$ and then IPTG (1 mM) and $CuSO_4$ (80 µM) were added to the culture, which was then incubated in a shaker overnight at 15 °C and 200 rpm. Cell harvesting was carried out by centrifugation at 6000 rpm, then the cells were re-suspended in 15 ml of lysis buffer (50 mM sodium phosphate, 300 mM NaCl, 10 mM imidazole, pH 8.0), lysed with a cell disruptor at 21 kpsi and then the cell lysate was centrifuged at 11,000 rpm for 30 min. The supernatant was loaded onto a nickel affinity column for immobilized metal affinity chromatography (IMAC), then the column was washed twice with wash buffer (50 mM sodium phosphate, 300 mM NaCl, 20 mM imidazole, pH 8.0), and the protein was eluted from the column with 5 ml of elution buffer (50 mM sodium phosphate, 300 mM NaCl, 250 mM imidazole, pH 8.0). The purified protein solution was treated with Tev protease to cleavage the poly His-tag and then subjected to a second IMAC. The native protein was desalted using a PD10 column and transferred to a 50 mM Tris, 150 NaCl buffer, pH 8.0. Protein quality was assayed by SDS-PAGE (see Figure 1A), using PageRuler Plus prestained protein ladder.

Enzyme Activity

The following laccase substrates were used: 2,2'-azino-bis(3-ethylbenzothiazoline-6-sulphonic acid) (ABTS, λ 420 nm); syringaldazine (SGZ, λ 530 nm); guiacol (λ 436 nm); 2,6-Dimethoxyphenol (2,6-DMP, λ 468 nm) and 2,4-Dichlorophenol (2,4-DCP, λ 510 nm) in presence of 4-amino antipyrine. Each substrate was used at 1 mM concentration, except SGZ, which was used at 0.05 mM concentration. Enzyme assays consisted of the substrate, a buffer (50 mM sodium acetate buffer pH 4.0 for ABTS and 2,6-DMP; or 50 mM sodium phosphate buffer pH 7.0 for SGZ, 2,4-DCP and guaiacol), enzyme (0.05 mg/mL) and $CuSO_4$ (0.5 mM). Activity was determined by following the absorbance change in a UV-Vis spectrophotometer, at the corresponding substrate wavelength. Steady state kinetic parameters were obtained for ABTS, SGZ and 2,6-DMP. One activity unit was defined as that amount of enzyme that catalyzes the conversion of 1 µmol of substrate per minute.

pH-activity profile was determined with ABTS and SGZ, under the same conditions as previously described in “enzyme activity” section, changing the buffer for a Britton and Robinson Universal buffer, in the range 2.3-10.4 [60]. Activity comparison and stability of

OcCueO was made with the commercial fungal *Trametes versicolor* laccase (TvL, ≥0.5 U/mg), purchased from Sigma-Aldrich, using ABTS and SGZ as substrates. For assessment of thermal stability at 50 ^{o}C, only ABTS (1 mM) was used as substrate in 50 mM sodium acetate buffer (pH 4.0) and in presence of $CuSO_4$ (0.5 mM).

Enzyme activity was also assayed with the lignin model compounds: β-aryl ether dimer guaiacylglycerol-β-guaiacyl (GGE), dissolved in methanol; and 2,2'-dihydroxy-3,3'-dimethoxy-5,5'-dicarboxybiphenyl (DDVA), dissolved in DMSO, as substrates. In this case, substrates were used at 2 mM concentration. Enzymatic reactions consisted of a substrate (GGE or DDVA), 20 mM ammonium bicarbonate buffer, enzyme (0.1 mg/mL) and $CuSO_4$ (0.5 mM). Reactions were carried out in presence and absence of ABTS (1mM) as mediator, overnight. The products were analyzed by HPLC and LC-MS.

Finally, enzyme activity was also analyzed with polymeric lignin, using eight different lignin preparations, including organosolv lignins, alkali lignins, lignosulfonate, and industrial Kraft lignin. Enzymatic reactions consisted of a polymeric lignin as substrate (5 mg), diluted in 1.2 mL of ammonium bicarbonate buffer (20 mM), enzyme (0.1 mg/mL) and $CuSO_4$ (0.5 mM). Reactions were performed in presence and absence of ABTS (1mM) and SGZ (0.05 mM) as mediators, overnight. Product formation was analyzed by HPLC and LC-MS.

HPLC and LC-MS assays

Products formed during reactions with lignin model compounds and polymeric lignin were analyzed by HPLC and LC-MS. Ethyl acetate (2 volumes) was added to the reaction mixture; then the sample was acidified with 100 µL of 1M HCl, gently mixed and the organic phase was collected and solvent removed in a rotary evaporator. Finally, the sample was re-suspended in 200 µL of 50% methanol, centrifuged and filtered for HPLC or LC-MS injection. HPLC analysis was performed using a Phenomenex Luna C_{18} reverse phase column (250 x 4.6 mm, 5 µ, 100 Å), on a Hewlett-Packard Series 1100 HPLC, and a Bruker Amazon X system for LC-MS. The set parameters were as follows: flow rate, 0.5 mL/min; wavelength, 270 nm; and gradient for which percentage is being referred to methanol (buffer B) in water (buffer A), 0-5% for 10 minutes, 5-10% for 10 minutes, 10-30% for 15 minutes, 30-40% for 5 minutes, 40-70% for 5 minutes, 70-100% for 15 minutes and 100-5% for 10 minutes, giving a total time of 70 minutes per run.

Crystallization, data collection, and structure

Pure recombinant OcCueO (10 mg/mL) in 20 mM sodium phosphate buffer pH 8, 100 mM NaCl was subjected to crystallisation screening using a Mosquito liquid handling robot (TTP Labtech). 200 nL of protein was mixed with 200 nL of crystallisation solution from commercially available screens in MRC 96-well 2-drop crystallisation plates (Molecular Dimensions). Plates were sealed with sealing films (EXCEL Scientific) and incubated at 22°C. Crystals appeared in a number of different conditions after 6-8 weeks. Rod shaped crystals were grown in condition B5 of the PactPremier crystallisation screen (Molecular Dimensions) containing 0.1 M MIB buffer pH 8, 25% PEG 1500. Crystals were removed from drops using a mounted Litholoop (Molecular Dimensions), cryoprotected in crystallisation solution containing 20% ethylene glycol, and flash-frozen in liquid nitrogen.

X-ray diffraction data to a resolution of 1.1 Å were collected at 100K at the beam line I03 at the Diamond Light Source, U.K. using a Pilatus 6M detector. All data were indexed, integrated and scaled using the XDS package [61]. Further data handling was carried out using the CCP4 software package [62]. The structure was solved by molecular replacement using the automated pipeline by BALBES [63]. Refinement of the structure was carried out by alternate cycles of manual refitting using Coot [64] and PHENIX [65]. Water molecules were added to the atomic model automatically using ARP [66], at the positions of large positive peaks in the difference electron density, only at places where the resulting water molecule fell into an appropriate hydrogen bonding environment. Restrained isotropic temperature factor refinements were carried out for each individual atom. The polypeptide chain was traced through electron density maps ($2F_o$ – F_c and F_o – F_c), except for residues 350-391. The structure was submitted to PDB-REDO [67] and then final manual refinements were made to the structure using Coot [64]. Data collection and refinement statistics are given in Table 1.

Site directed mutagenesis (SDM)

With the aim to identify and study similarities and differences between fungal and bacterial laccases, a protein search was carried out in Uniprot (http://www.uniprot.org/) and NCBI (https://www.ncbi.nlm.nih.gov/protein/) databases. A total of 32 fungal laccases and 33 bacterial laccases or multicopper oxidases, putative and annotated, were selected. A multiple sequence alignment was performed using the CLC workbench software (https://www.qiagenbioinformatics.com/). Target amino acids for site directed mutagenesis (SDM) were selected and divided into two groups (see Table 5), group 1 was based on highly conserved amino acids among all fungal and bacterial laccases; while group 2 was based on conserved amino acids nearby copper atoms that appear only in high redox potential fungal

laccases (HRPL). In both cases, the reported well-known copper binding amino acids in laccases: HXHG, HXH, HXXHXH and HCHXXXHXXXXM/L/F [45], were excluded. Site directed mutagenesis (SDM) was carried out using the QuikChange II XL Site-Directed Mutagenesis Kit (Agilent), following the instructions provided by the manufacturer. A total of 8 mutants were evaluated. Mutants 1, 2, 3, 4 and 8 belonged to group 1, while mutants 5, 6, and 7 belonged to group 2. The oligonucleotide primers and a list of the mutated residues can be found in Table 2.

Acknowledgements

This work was supported by BBSRC research grants BB/M025772/1, BB/M003523/1, and BB/P01738X/1, and FMS is supported by FAPESP research grant 2015/50590-4. RSGT was supported by a PhD studentship funded by Secretaria de Educacion Superior, Ciencia, Tecnologia e Innovacion (SENESCYT), Ecuador. Crystallographic data were collected at Diamond Light Source, UK and we acknowledge the support of the beam line scientist Dr David Hall. We thank Dr. Freddy Tjosås (Borregaard) for provision of samples of Ca-lignosulfonate.

Author contributions

TDHB, FS, VF planned the research. RSGT performed the CueO enzymology research, RW performed the protein crystallography research, and GFP performed the genome sequencing research. All authors analysed the data and contributed towards writing the paper.

Conflict of interest.

The authors declare no conflict of interest.

References

1. Leonowicz, A., Matuszewska, A., Luterek, J., Ziegenhagen, D., Wojtaś-Wasilewska, M., Cho, N.-S., Hofrichter, M. & Rogalski, J. (1999) Biodegradation of lignin by white rot fungi, *Fungal Gen. Biol..* **27**, 175-185.

2. Millati, R., Syamsiah, S., Niklasson, C., Cahyanto, M. N., Ludquist, K. & Taherzadeh, M. J. (2011) Biological pretreatment of lignocelluloses with white-rot fungi and its applications: a review, *BioResources.* **6**, 5224-5259.

3. Brown, M. E. & Chang, M. C. (2014) Exploring bacterial lignin degradation, *Curr. Opin. Chem. Biol..* **19**, 1-7.

4. Bugg, T. D. H., Ahmad, M., Hardiman, E. M. & Singh, R. (2011) The emerging role for bacteria in lignin degradation and bio-product formation, *Curr. Opin. Biotech.* **22**, 394-400.

5. Ahmad, M., Roberts, J. N., Hardiman, E. M., Singh, R., Eltis, L. D. & Bugg, T. D. H. (2011) Identification of DypB from *Rhodococcus jostii* RHA1 as a lignin peroxidase, *Biochemistry.* **50**, 5096-5107.

6. Brown, M. E., Barros, T. & Chang, M. C. (2012) Identification and characterization of a multifunctional dye peroxidase from a lignin-reactive bacterium, *ACS Chem. Biol.* **7**, 2074-2081.

7. Rahmanpour, R. & Bugg, T. D. H. (2015) Characterisation of Dyp-type peroxidases from *Pseudomonas fluorescens* Pf-5: Oxidation of Mn(II) and polymeric lignin by Dyp1B, *Arch. Biochem. Biophys.* **574**, 93-98.

8. Lin, L., Cheng, Y., Pu, Y., Sun, S., Li, X., Jin, M., Pierson, E. A., Gross, D. C., Dale, B. E. & Dai, S. Y. (2016) Systems biology-guided biodesign of consolidated lignin conversion, *Green Chem.* **18**, 5536-5547.

9. Morozova, O. V., Shumakovich, G. P., Gorbacheva, M. A., Shleev, S. V. & Yaropolov, A. I. (2007) "Blue" laccases, *Biochemistry Moscow.* **72**, 1136-1150.

10. Pezzella, C., Guarino, L. & Piscitelli, A. (2015) How to enjoy laccases, *Cell Mol Life Sci.* **72**, 923-940.

11. Munk, L., Sitarz, A. K., Kalyani, D. C., Mikkelsen, J. D. & Meyer, A. S. (2015) Can laccases catalyze bond cleavage in lignin?, *Biotechnol. Adv.* **33**, 13-24.

12. Majumdar, S., Lukk, T., Solbiati, J. O., Bauer, S., Nair, S. K., Cronan, J. E. & Gerlt, J. A. (2014) Roles of small laccases from *Streptomyces* in lignin degradation, *Biochemistry.* **53**, 4047-4058.

13. Sharma, P., Goel, R. & Capalash, N. (2007) Bacterial laccases, *World J. Microbiol. Biotechnol.* **23**, 823-832.

14. Hullo, M.-F., Moszer, I., Danchin, A. & Martin-Verstraete, I. (2001) CotA of *Bacillus subtilis* Is a copper-dependent laccase, *J. Bacteriol.* **183**, 5426-5430.
15. Roberts, S. A., Weichsel, A., Grass, G., Thakali, K., Hazzard, J. T., Tollin, G., Rensing, C. & Montfort, W. R. (2002) Crystal structure and electron transfer kinetics of CueO, a multicopper oxidase required for copper homeostasis in *Escherichia coli*, *Proc. Natl. Acad. Sci. USA* **99**, 2766-2771.
16. Grass, G. & Rensing, C. (2001) CueO Is a multi-copper oxidase that confers copper tolerance in *Escherichia coli*, *Biochem. Biophys. Res. Commun.* **286**, 902-908.
17. Ausec, L., Zakrzewski, M., Goesmann, A., Schlüter, A. & Mandic-Mulec, I. (2011) Bioinformatic analysis reveals high diversity of bacterial genes for laccase-like enzymes, *PLoS One.* **6**, e25724.
18. Martins, L. O., Soares, C. M., Pereira, M. M., Teixeira, M., Costa, T., Jones, G. H. & Henriques, A. O. (2002) Molecular and biochemical characterization of a highly stable bacterial laccase that occurs as a structural component of the *Bacillus subtilis* endospore coat, *J. Biol. Chem.* **277**, 18849-18859.
19. Reiss, R., Ihssen, J. & Thöny-Meyer, L. (2011) *Bacillus pumilus* laccase: a heat stable enzyme with a wide substrate spectrum, *BMC Biotechnol.* **11**, 1.
20. Brander, S., Mikkelsen, J. D. & Kepp, K. P. (2014) Characterization of an alkali-and halide-resistant laccase expressed in *E. coli*: CotA from *Bacillus clausii, PLoS One.* **9**, e99402.
21. Koschorreck, K., Richter, S. M., Ene, A. B., Roduner, E., Schmid, R. D. & Urlacher, V. B. (2008) Cloning and characterization of a new laccase from *Bacillus licheniformis* catalyzing dimerization of phenolic acids, *Appl. Microbiol. Biotechnol.* **79**, 217-224.
22. Dubé, E., Shareck, F., Hurtubise, Y., Daneault, C. & Beauregard, M. (2008) Homologous cloning, expression, and characterisation of a laccase from *Streptomyces coelicolor* and enzymatic decolourisation of an indigo dye, *Appl. Microbiol. Biotechnol.* **79**, 597-603.
23. Gunne, M. & Urlacher, V. B. (2012) Characterization of the alkaline laccase Ssl1 from *Streptomyces sviceus* with unusual properties discovered by genome mining, *PLoS One.* **7**, e52360.
24. Kalyani, D., Munk, L., Mikkelsen, J. & Meyer, A. (2016) Molecular and biochemical characterization of a new thermostable bacterial laccase from *Meiothermus ruber* DSM 1279, *RSC Adv.* **6**, 3910-3918.
25. Li, X., Wei, Z., Zhang, M., Peng, X., Yu, G., Teng, M. & Gong, W. (2007) Crystal structures of *E. coli* laccase CueO at different copper concentrations, *Biochem. Biophys. Res. Commun.* **354**, 21-26.

26. Ihssen, J., Reiss, R., Luchsinger, R., Thöny-Meyer, L. & Richter, M. (2015) Biochemical properties and yields of diverse bacterial laccase-like multicopper oxidases expressed in *Escherichia coli, Scientific reports.* **5**, article 10465.
27. Durao, P., Chen, Z., Fernandes, A. T., Hildebrandt, P., Murgida, D. H., Todorovic, S., Pereira, M. M., Melo, E. P. & Martins, L. O. (2008) Copper incorporation into recombinant CotA laccase from *Bacillus subtilis*: characterization of fully copper loaded enzymes, *J. Biol. Inorg. Chem.* **13**, 183-193.
28. Taylor, C. R., Hardiman, E. M., Ahmad, M., Sainsbury, P. D., Norris, P. R. & Bugg, T. D. H. (2012) Isolation of bacterial strains able to metabolize lignin from screening of environmental samples, *J. Appl. Microbiol.* **113**, 521-530.
29. Rashid, G. M., Duran-Pena, M. J., Rahmanpour, R., Sapsford, D. & Bugg, T. D. (2017) Delignification and enhanced gas release from soil containing lignocellulose by treatment with bacterial lignin degraders, *J. Appl. Microbiol* **123**, 159-171.
30. Rashid, G. M., Taylor, C. R., Liu, Y., Zhang, X., Rea, D., Fülöp, V. & Bugg, T. D. (2015) Identification of manganese superoxide dismutase from *Sphingobacterium* sp. T2 as a novel bacterial enzyme for lignin oxidation, *ACS Chem. Biol.* **10**, 2286-2294.
31. Sainsbury, P. D., Hardiman, E. M., Ahmad, M., Otani, H., Seghezzi, N., Eltis, L. D. & Bugg, T. D. (2013) Breaking down lignin to high-value chemicals: the conversion of lignocellulose to vanillin in a gene deletion mutant of Rhodococcus jostii RHA1, *ACS Chem. Biol.* **8**, 2151-2156.
32. Mycroft, Z., Gomis, M., Mines, P., Law, P. & Bugg, T. D. (2015) Biocatalytic conversion of lignin to aromatic dicarboxylic acids in Rhodococcus jostii RHA1 by re-routing aromatic degradation pathways, *Green Chemistry.* **17**, 4974-4979.
33. Piontek, K., Antorini, M. & Choinowski, T. (2002) Crystal structure of a laccase from the fungus *Trametes versicolor* at 1.90-Å resolution containing a full complement of coppers, *J. Biol. Chem.* **277**, 37663-37669.
34. Ferraroni, M., Myasoedova, N. M., Schmatchenko, V., Leontievsky, A. A., Golovleva, L. A., Scozzafava, A. & Briganti, F. (2007) Crystal structure of a blue laccase from *Lentinus tigrinus*: evidences for intermediates in the molecular oxygen reductive splitting by multicopper oxidases, *BMC Structural Biology.* **7**, 60.
35. Baker, E. N. (1988) Structure of azurin from *Alcaligenes denitrificans* refinement at 1· 8 Å resolution and comparison of the two crystallographically independent molecules, *J. Mol. Biol.* **203**, 1071-1095.
36. Sakurai, T. & Kataoka, K. (2007) Structure and function of type I copper in multicopper oxidases, *Cell Mol Life Sci.* **64**, 2642-2656.

37. Ducros, V., Brzozowski, A. M., Wilson, K. S., Brown, S. H., Østergaard, P., Schneider, P., Yaver, D. S., Pedersen, A. H. & Davies, G. J. (1998) Crystal structure of the type-2 Cu depleted laccase from *Coprinus cinereus* at 2.2 Å resolution, *Nat. Struct. Mol. Biol.* **5**, 310-316.
38. O'Neill, P., Stevens, D. L. & Garman, E. F. (2002) Physical and chemical considerations of damage induced in protein crystals by synchrotron radiation: a radiation chemical perspective. *J. Synchrotron Radiation.* **9**, 329-332.
39. Komori, H. & Higuchi, Y. (2015) Structural insights into the O_2 reduction mechanism of multicopper oxidase, *J. Biochem.* **158**, 293-298.
40. Kataoka, K., Komori, H., Ueki, Y., Konno, Y., Kamitaka, Y., Kurose, S., Tsujimura, S., Higuchi, Y., Kano, K. & Seo, D. (2007) Structure and function of the engineered multicopper oxidase CueO from *Escherichia coli*—deletion of the methionine-rich helical region covering the substrate-binding site, *J. Mol. Biol.* **373**, 141-152.
41. Pieper, U., Eswar, N., Davis, F. P., Braberg, H., Madhusudhan, M. S., Rossi, A., Marti-Renom, M., Karchin, R., Webb, B. M. & Eramian, D. (2006) MODBASE: a database of annotated comparative protein structure models and associated resources. *Nucl. Acids Res.* **34**, D291-D295.
42. Petřek, M., Otyepka, M., Banáš, P., Košinová, P., Koča, J. & Damborský, J. (2006) CAVER: a new tool to explore routes from protein clefts, pockets and cavities, *BMC Bioinformatics.* **7**, 316.
43. Hakulinen, N., Andberg, M., Kallio, J., Koivula, A., Kruus, K. & Rouvinen, J. (2008) A near atomic resolution structure of a Melanocarpus albomyces laccase, *J. Struct. Biol.* **162**, 29-39.
44. Messerschmidt, A., Ladenstein, R., Huber, R., Bolognesi, M., Avigliano, L., Petruzzelli, R., Rossi, A. & Finazzi-Agró, A. (1992) Refined crystal structure of ascorbate oxidase at 1.9 Å resolution, *J. Mol. Biol.* **224**, 179-205.
45. Kumar, S., Phale, P. S., Durani, S. & Wangikar, P. P. (2003) Combined sequence and structure analysis of the fungal laccase family. *Biotech. Bioeng.* **83**, 386-394.
46. Mate, D. M. & Alcalde, M. (2015) Laccase engineering: From rational design to directed evolution, *Biotechnol. Adv.* **33**, 25-40.
47. Kiiskinen, L.-L. & Saloheimo, M. (2004) Molecular cloning and expression in Saccharomyces cerevisiae of a laccase gene from the ascomycete *Melanocarpus albomyces*, *Appl. Environ. Microbiol.* **70**, 137-144.
48. Liu, W., Chao, Y., Liu, S., Bao, H. & Qian, S. (2003) Molecular cloning and characterization of a laccase gene from the basidiomycete *Fome lignosus* and expression in *Pichia pastoris*, *Appl. Microbiol. Biotechnol.* **63**, 174-181.

49. Kiiskinen, L.-L., Kruus, K., Bailey, M., Ylösmäki, E., Siika-aho, M. & Saloheimo, M. (2004) Expression of Melanocarpus albomyces laccase in *Trichoderma reesei* and characterization of the purified enzyme, *Microbiology.* **150**, 3065-3074.
50. Kirk, T. K. & Farrell, R. L. (1987) Enzymatic" combustion": the microbial degradation of lignin, *Annu. Rev. Microbiol.* **41**, 465-501.
51. Durão, P., Bento, I., Fernandes, A. T., Melo, E. P., Lindley, P. F. & Martins, L. O. (2006) Perturbations of the T1 copper site in the CotA laccase from *Bacillus subtilis*: structural, biochemical, enzymatic and stability studies, *J. Biol. Inorg. Chem.* **11**, 514.
52. Orlikowska, M., Rostro-Alanis, M.J., Bujacz, A., Hernandez-Luna, C., Rubio, R., Parra, R., and Bujacz, G. (2018) Structural studies of two thermostable laccases from the white-rot fungus Pycnoporus sanguineus. *Int. J. Biol. Macromol.* **107B**, 1629-1640.
53. Bugg, T. D. H. & Rahmanpour, R. (2015) Enzymatic conversion of lignin into renewable chemicals, *Curr. Opin. Chem. Biol.* **29**, 10-17.
54. Martinez, D., Larrondo, L. F., Putnam, N., Gelpke, M. D. S., Huang, K., Chapman, J., Helfenbein, K. G., Ramaiya, P., Detter, J. C. & Larimer, F. (2004) Genome sequence of the lignocellulose degrading fungus *Phanerochaete chrysosporium* strain RP78, *Nature Biotech.* **22**, 695-700.
55. Ohm, R. A., De Jong, J. F., Lugones, L. G., Aerts, A., Kothe, E., Stajich, J. E., De Vries, R. P., Record, E., Levasseur, A. & Baker, S. E. (2010) Genome sequence of the model mushroom *Schizophyllum commune*, *Nature Biotech.* **28**, 957-963.
54. Bolger, A. M., Lohse, M. & Usadel, B. (2014) Trimmomatic: a flexible trimmer for Illumina sequence data, *Bioinformatics.* **30**, 2114-2120.
55. Bankevich, A., Nurk, S., Antipov, D., Gurevich, A. A., Dvorkin, M., Kulikov, A. S., Lesin, V. M., Nikolenko, S. I., Pham, S. & Prjibelski, A. D. (2012) SPAdes: a new genome assembly algorithm and its applications to single-cell sequencing, *J. Comp. Biol.* **19**, 455-477.
56. Wang, Z. & Wu, M. (2013) A phylum-level bacterial phylogenetic marker database, *Mol. Biol. Evol.* **30**, 1258-1262.
57. Besemer, J. & Borodovsky, M. (2005) GeneMark: web software for gene finding in prokaryotes, eukaryotes and viruses, *Nucl. Acids Res.* **33**, W451-W454.
58. Seemann, T. (2014) Prokka: rapid prokaryotic genome annotation, *Bioinformatics.* **30**, 2068-2069.
59. Yoon, S.-H., Ha, S.-M., Kwon, S., Lim, J., Kim, Y., Seo, H. & Chun, J. (2017) Introducing EzBioCloud: a taxonomically united database of 16S rRNA gene sequences and whole-genome assemblies, *Int. J. Syst. Evol. Microbiol.* **67**, 1613-1617.

60. Britton, H. T. S. & Robinson, R. A. (1931) Universal buffer solutions and the dissociation constant of veronal, *J. Chem. Soc.*, 1456-1462.
61. Kabsch, W. (2010) Xds, *Acta Cryst.* **D66**, 125-132.
62. Dodson, E. J., Winn, M. & Ralph, A. (1997) Collaborative computational project, number 4: Providing programs for protein crystallography, *Meth. Enzymol.* **277**, 620-633.
63. Long, F., Vagin, A. A., Young, P. & Murshudov, G. N. (2008) BALBES: a molecular-replacement pipeline, *Acta Cryst.* **D64**, 125-132.
64. Emsley, P. & Cowtan, K. (2004) Coot: model-building tools for molecular graphics, *Acta Cryst..* **D60**, 2126-2132.
65. Adams, P. D., Afonine, P. V., Bunkóczi, G., Chen, V. B., Davis, I. W., Echols, N., Headd, J. J., Hung, L.-W., Kapral, G. J. & Grosse-Kunstleve, R. W. (2010) PHENIX: a comprehensive Python-based system for macromolecular structure solution, *Acta Cryst.* **D66**, 213-221.
66. Langer, G. G., Cohen, S. X., Lamzin, V. S. & Perrakis, A. (2008) Automated macromolecular model building for X-ray crystallography using ARP/wARP version 7, *Nat. Protocols.* **3**, 1171.
67. Joosten, R. P., Long, F., Murshudov, G. N. & Perrakis, A. (2014) The PDB_REDO server for macromolecular structure model optimization, *IUCrJ.* **1**, 213-220.
68. L. Delano, W. (2002) *The PyMol user's manual*.

Table 1. Steady-state kinetic constants for OcCueO

Substrate	**Km [μM]**	**Vmax [U/mg protein]**	**kcat [s^{-1}]**	**Specificity constant kcat/Km [s^{-1} M^{-1}]**
ABTS	1463	1.0	0.93	635.8
SGZ	4	0.5	0.46	110594.8
2,6-DMP	307	0.9	0.9	2929.9

Table 2. Characteristics of solvent channels calculated for OcCueO.

Putative Solvent Channel	Throughput	Cost	Length/ Å	Curvature	Bottleneck radius	Bottleneck residues
1	0.44	0.82	25.00	1.34	1.35	H131, L493, H491, T138, P132, E496, H133, W129, H489, A142, H93
2	0.27	1.31	30.82	1.5	0.93	V186, F198, R179, V180, H143, Y187, R178, E188
3	0.68	0.38	12.6	1.2	1.4	H91, W92, H93, G94, L95, D102, H437, I438, H439, G440, D462, R478

Throughput – denotes ease with which compounds could pass through the tunnel.
Cost – the cost function denotes how likely a tunnel is with short direct paths 'cheap' and long complicated paths 'expensive'.
Curvature – is the length of the tunnel divided by the shortest distance of the origin to the tunnel end point.
Bottleneck radius – the radius for the smallest part of the tunnel.

Table 3. Well-conserved residues among bacterial and fungal laccases (Group 1) and well-conserved residues in HRPL near to copper atoms and absent in bacterial laccases (Group 2).

Group 1: Well-conserved residues among bacterial and fungal laccases		**Group 2: Well-conserved residues in HRPL near to copper atoms and absent in bacterial laccases**	
OcCueO location	**Alignment hit percentage among fungal and bacterial laccases**	**OcCueO location**	**Well-conserved HRPL sequence**
D (102)	98 %	K (482), S (483) H (484) and F (486)	NPG - W
G (103)	91%		
R (221)	91 %		
R (223)	97 %		
D (249)	94 %	I (109), A (110), A (111) and G (112)	QCPI
R (269)	92%		
D (462)	95%		
G (145)	100%		
D (177)	94%		

Table 1. Summary of crystallographic data collection and refinement statistics

Data collection	
Wavelength (Å)	0.8
Unit cell (*a, b, c*) (Å), (β) (°)	47.33, 48.31, 88.85, 93.78
Space group	$P2_1$
Resolution (Å)	89-1.1 (1.16-1.1)
Observations	602,426
Unique reflections	161,992
I/σ(I)	12.2 (2.1)
R_{sym}[a]	0.056 (0.584)
Completeness (%)	99.9 (99.7)
$CC_{1/2}$[b]	0.999 (0.748)
Refinement	
Non-hydrogen atoms	3,918 (including Cu^{2+}, 2 ethylene glycol & 477 water molecules)
R_{cryst}[c]	0.125 (0.242)
Reflections used	155,475 (11,395)
R_{free}[d]	0.149 (0.246)
Reflections used	6,517 (493)
R_{cryst} (all data)[b]	0.126
Average temperature factors (Å^2)	
All atoms	14.1
Protein	12.4
Water	23.5
From Wilson plot	9.1
Rmsds from ideal values	
Bonds (Å)	0.019
Angles (°)	1.8
DPI coordinate error (Å)[e]	0.02
Ramachandran Plot (%)	
Most favoured	97
Additional allowed	3
Outliers	0
wwPDB code	

Numbers in parentheses refer to values in the highest resolution shell.

[a] $R_{sym} = \Sigma_j\Sigma_h|I_{h,j} - \langle I_h\rangle|/\Sigma_j\Sigma_h\langle I_h\rangle$ where $I_{h,j}$ is the jth observation of reflection h, and $\langle I_h\rangle$ is the mean intensity of that reflection

[b] $CC_{1/2}$ is the correlation coefficient of the mean intensities between two random half-sets of data

[c] $R_{cryst} = \Sigma||F_{obs}|-|F_{calc}||/\Sigma|F_{obs}|$ where F_{obs} and F_{calc} are the observed and calculated structure factor amplitudes, respectively

[d] R_{free} is equivalent to R_{cryst} for a 4% subset of reflections not used in the refinement

[e] DPI refers to the diffraction component precision index [Cruckshank]

Table 2. List of target mutations and primers used for Site Directed mutagenesis.

Mutant	Native residues	Mutant residues	Forward and reverse primers 5' – 3'
1	K, D (461, 462)	A, A	Fw cgcatcaatcgggatgggcggctaccgcattgatcgacg Rev cgtcgatcaatgcggtagccgcccatcccgattgatgcg
2	R-R (221, 223)	A-A	Fw ccctgcatctatcgtcgctctggctatcttgaacggcgcc Rev ggcgccgttcaagatagccagagcgacgatagatgcaggg
3	D, G (102, 103)	A, A	Fw gccgtcgatactcgctgccggaccccataatg Rev cattatggggtccggcagcgagtatcgacggc
4	S, F, N (126-128)	G, T, F	Fw gaagtcaaaattcagcaaccggctgggaccttctggttccatccgcatttgcacgg Rev ccgtgcaaatgcggatggaaccagaaggtcccagccggttgctgaattttgacttc
5	I, A, A (109-111)	Q, C, P	Fw gtcgatactcgatggcggaccccataatgttcagtgcccgggcgaggcttggaa Rev ttccaagcctcgcccgggcactgaacattatggggtccgccatcgagtatcgac
6	F, M (486, 487)	W, L	Fw gtgaggcggtgaaaagccatccatggttgtttcattgccatgttctg Rev cagaacatggcaatgaaacaaccatggatggcttttcaccgcctcac
7	K, S, H (482-484)	N, P, G	Fw ctggttcattttgaccgtgaggcggtgaatcccggtccatttatgtttcattgcca Rev tggcaatgaaacataaatggaccgggattcaccgcctcacggtcaaaatgaaccag
8	K (461)	R	Fw gcgcatcaatcgggatggcgcgataccgcattgatcgac Rev gtcgatcaatgcggtatcgcgccatcccgattgatgcgc

Figure Legends.

Figure 1. UV–Visible absorption spectra of purified recombinant OcCueO (0·5 mg/mL), in 50 mM Tris buffer pH 7.5.

Figure 2. Kinetic analysis of recombinant OcCueO and comparison with fungal laccase. (A) OcCueO pH-activity profile with ABTS and SGZ. (B) Relative comparison of kinetic efficiency between bacterial laccase OcCueO and fungal laccase TvL, with ABTS and SGZ as substrates. (C) Stability comparison between bacterial laccase OcCueO and fungal laccase TvL, with ABTS as substrate.

Figure 3. Reaction products obtained from incubation of OcCueO with lignin model compounds GGE (Panel A), DDVA (Panel B), and Ca-lignosulfonate lignin (Panel C). For (A) and (B), *m/z* values for products and substrate are shown. In the mini-photo (from left to right), the final reaction mixture of: blank, OcCueO, blank with ABTS as mediator and OcCueO with ABTS as mediator.

Figure 4. Structure of *Ochrobactrum* laccase (OcCueO), with protein surface shown. The three domains are coloured in dark blue (domain 1), light blue (domain 2) and grey (domain 3). Figure was constructed with PyMol [68] for Protein Data Bank (PDB) data, 6EVG.

Figure 5. Comparison of T1 copper sites from *Ochrobactrum* CueO, *E. coli* CueO (PDB: 1KV7) and *Trametes versicolor laccase* (PDB: 1GYC). (A) *Ochrobactrum* CueO T1 site with trigonal pyramidal co-ordination of the copper ion. Residues involved in co-ordinating copper are depicted as green stick models. The $2F_o - F_C$ electron density map (1.5 σ level) around each of these residues and the copper is represented by grey mesh. Dashed black lines represent the distances between co-ordinating residues and the copper (shown as a sphere). (B) *E. coli* CueO T1 site, with trigonal pyramidal co-ordination of the copper ion. Residues involved in co-ordinating copper are depicted as green stick models. Dashed black lines represent the distances between co-ordinating residues and the copper. (C) TvL laccase T1 site, with trigonal coplanar co-ordination of the copper ion. Residues involved in co-ordinating copper are depicted as green stick models. Dashed black lines represent the distances between co-ordinating residues and the copper (shown as a sphere).

Figure 6. OcCueO T2/3 site. (A) OcCueO T2/3 site conserved histidines are depicted as green stick models. The $2F_o - F_c$ electron density map (1.5 σ level) around each of the conserved histidines is represented as grey mesh. (B) OcCueO T2/3 site with modelled copper ions (shown as spheres) based on co-ordinates from *E. coli* CueO (PDB: 3NSF) which shared highest sequence similarity. Conserved histidines are again depicted as green stick models and the $2F_o - F_C$ electron density map (1.5 σ level) represented as grey mesh. (C) Superposition of the *E. coli* CueO (PDB: 1KV7) T2/3 site conserved histidines (dark grey) onto the apo OcCueO T2/3 site conserved histidines (green). Residue labels refer to the conserved histidines in OcCueO.

Figure 7. Location of conserved residues amongst bacterial and fungal laccase in respect to accessible paths to copper atoms, identified by CAVER [55]. OcCueO is represented as a ribbon diagram with conserved residues depicted as green stick models and T1, T2 and T3 copper ions are depicted as copper spheres. (A) Paths from T3 side of the T2/3 copper site are shown as either blue or red mesh, with water molecules shown as grey spheres and start point for the tunnels shown as a white sphere. (B) Path from T2 side of the T2/3 copper site is shown as a blue mesh. Figure was constructed with PyMol [68] for Protein Data Bank (PDB) data, 6EVG.

Figure 8.

Partial amino acid sequence alignment, showing 10 bacterial laccase-like multicopper oxidases (in gray background) and 10 fungal laccases. Metal-binding residues are coloured in blue; other conserved residues are coloured in red (see Table 5), while mismatches are highlighted in yellow. Numbering is based on OcCueO sequence as reference. Uniprot or GenBank accession codes as follows: 2, P07788; 3, P36649; 4, A0A0E0XT94; 5, (GB) WP_011709064.1; 6, Q88C03; 7, B9W2C5; 8, (GB) WP_013012601.1; 9, P12374; 10, E1ACR6; 11, Q12718; 12, D0VWU3; 13, Q12739; 14, Q12571; 15, Q12541; 16, Q9HDQ0; 17, Q12570; 18, P06811; 19, Q70KY3; and 20, E9RBR0.

Figure 9

Kinetic activity of OcCueO mutants with ABTS and SGZ as substrates.

Figure 1.

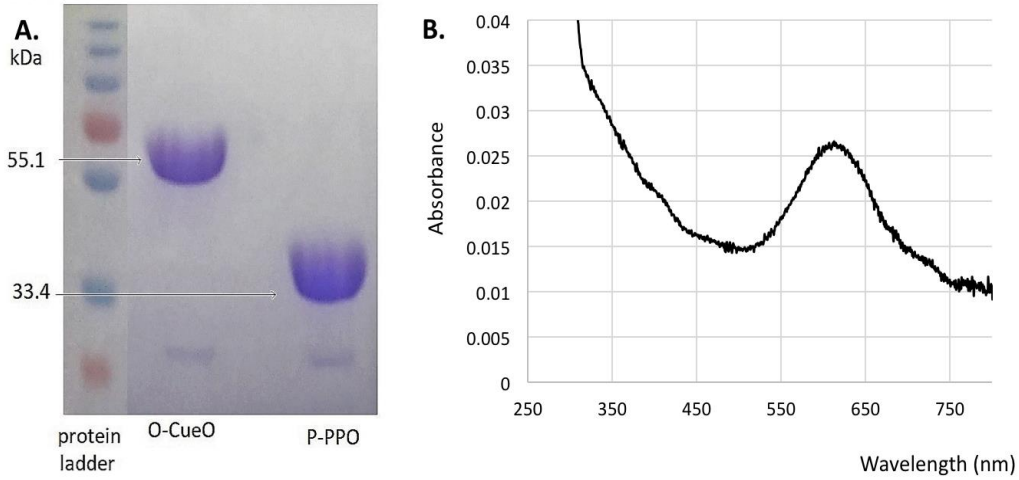

Figure 2.

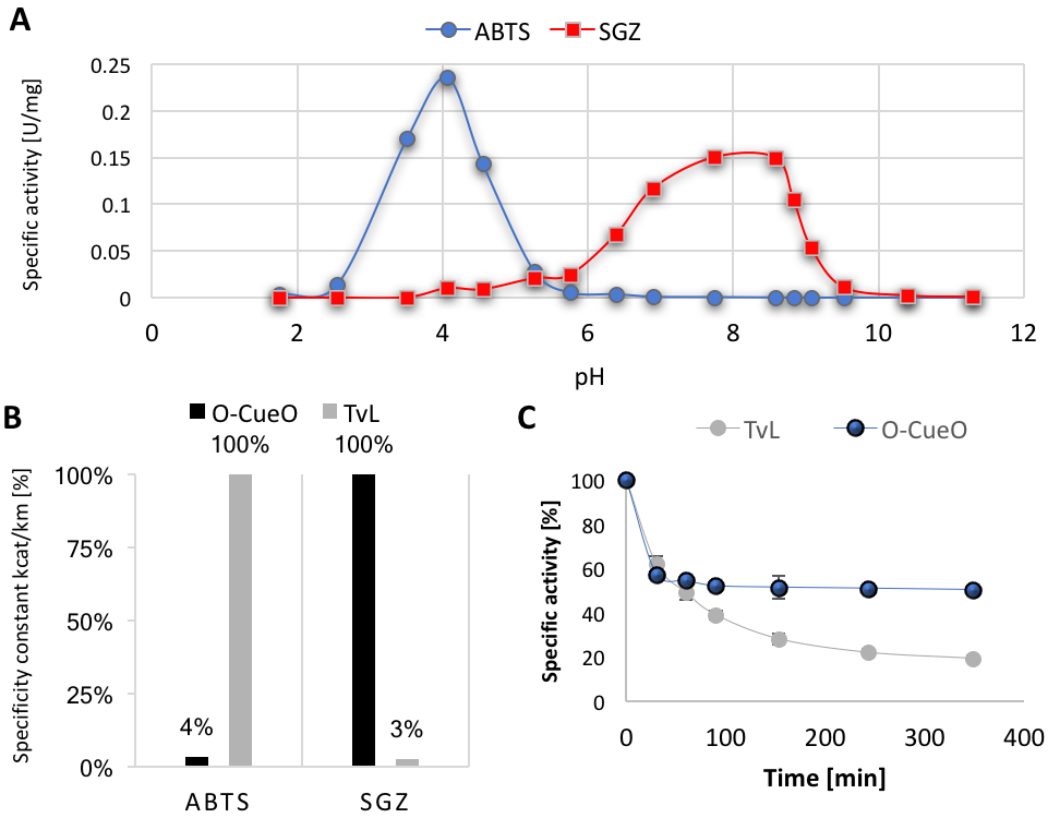

Figure 3.

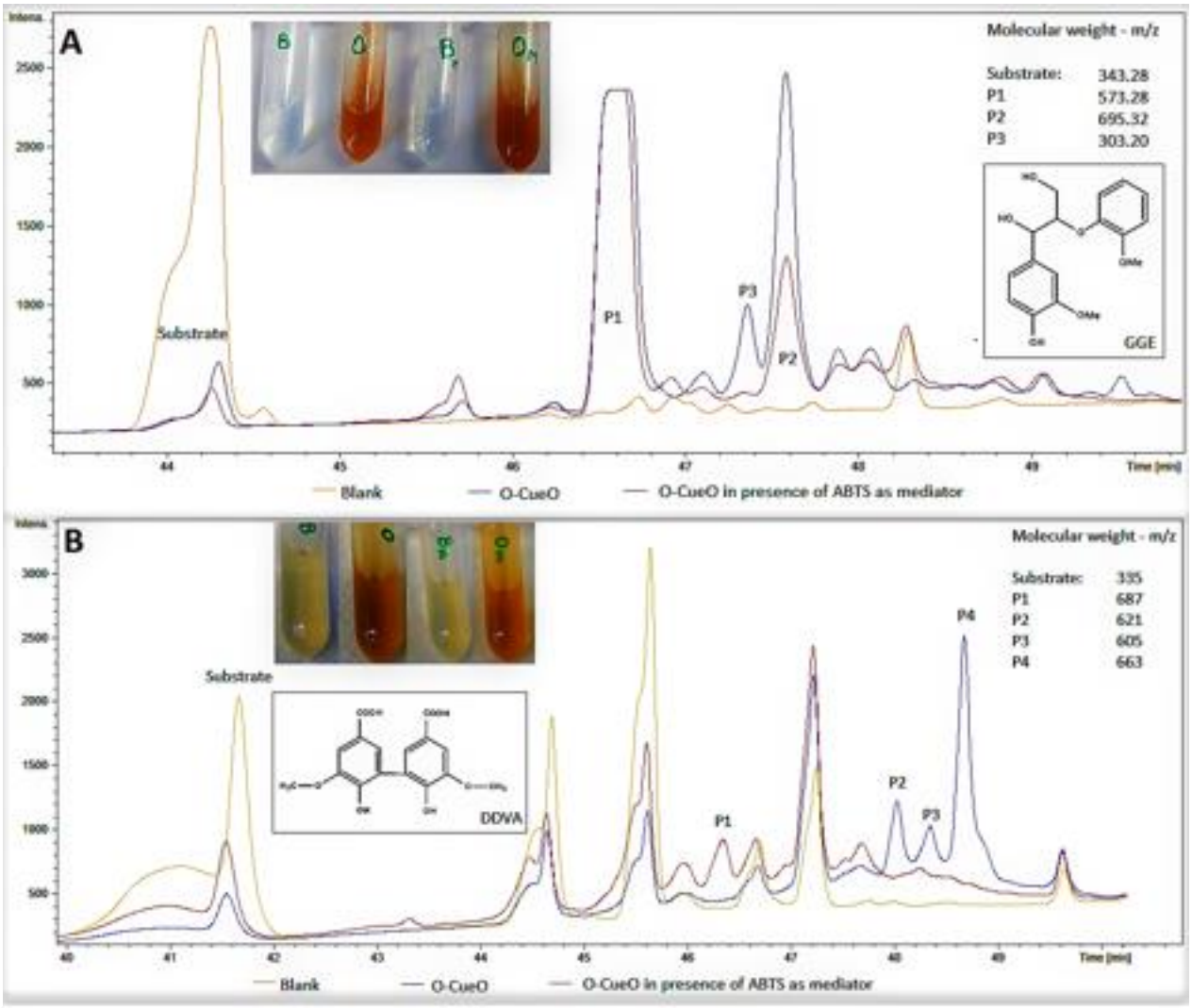
A
Molecular weight - m/z
Substrate: 343.28
P1 573.28
P2 695.32
P3 303.20
GGE
Substrate
P1
P2
P3
Time [min]
Blank
O-CueO
O-CueO in presence of ABTS as mediator
B
Molecular weight - m/z
Substrate: 335
P1 687
P2 621
P3 605
P4 663
DDVA
Substrate
P1
P2
P3
P4
Time [min]
Blank
O-CueO
O-CueO in presence of ABTS as mediator

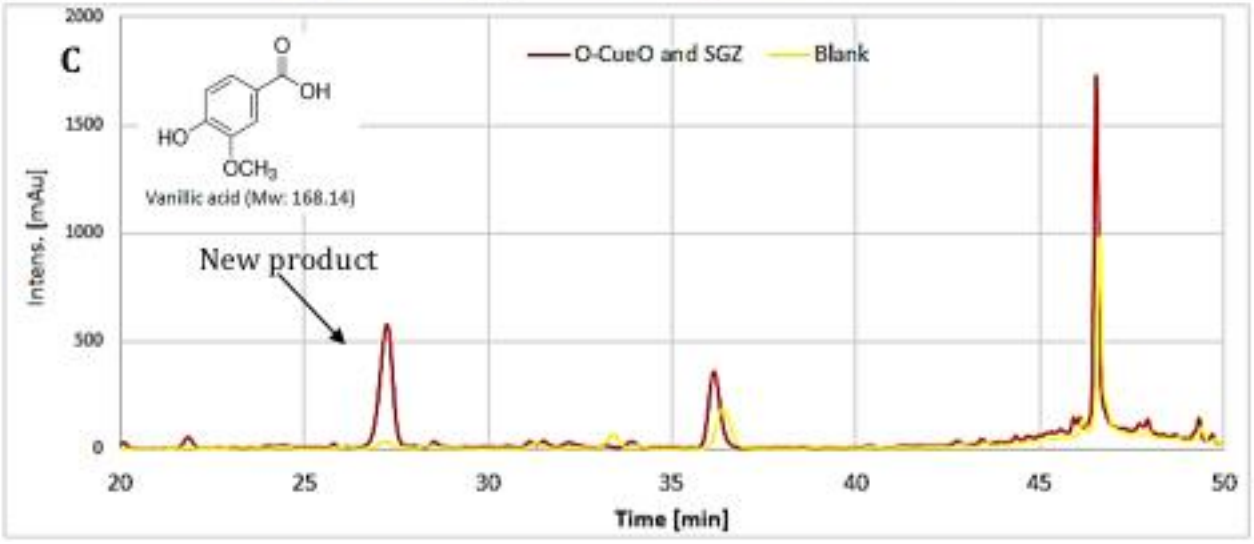
C
O-CueO and SGZ
Blank
Vanillic acid (Mw: 168.14)
New product
Intens. [mAu]
Time [min]

Figure 4

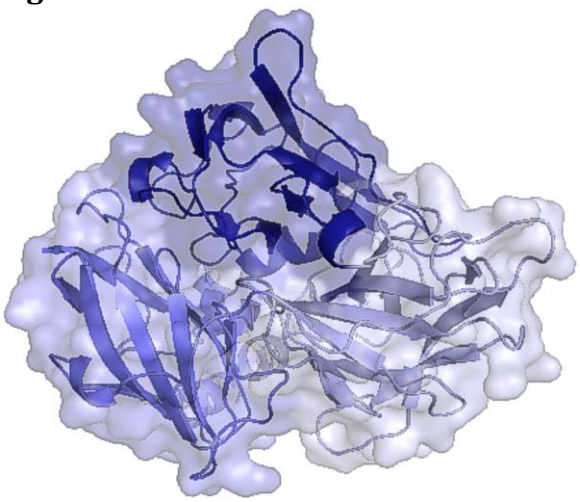

Figure 5

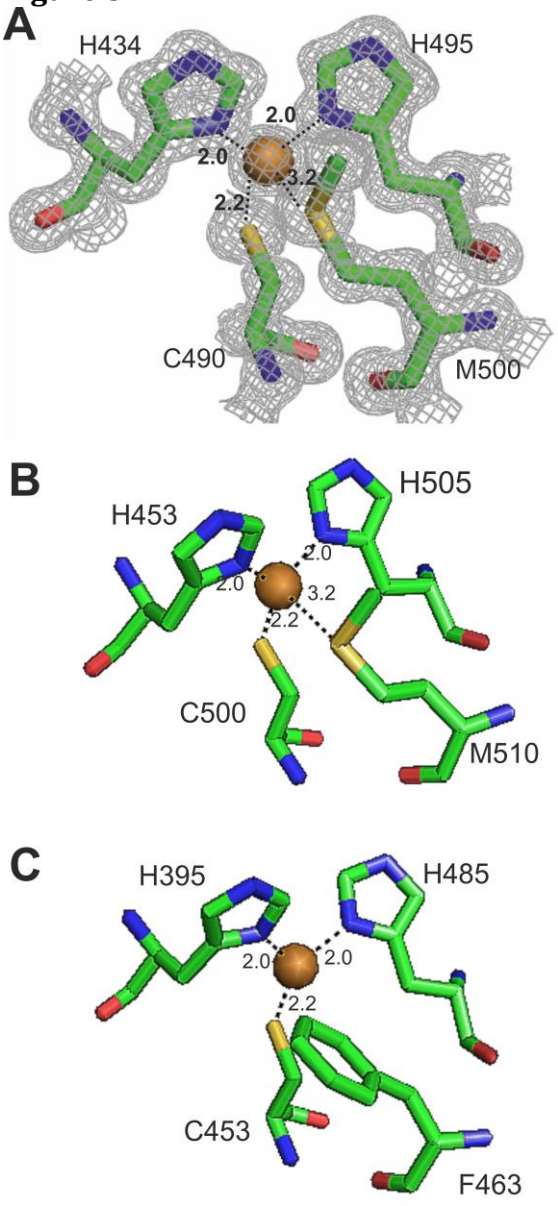

Figure 6.

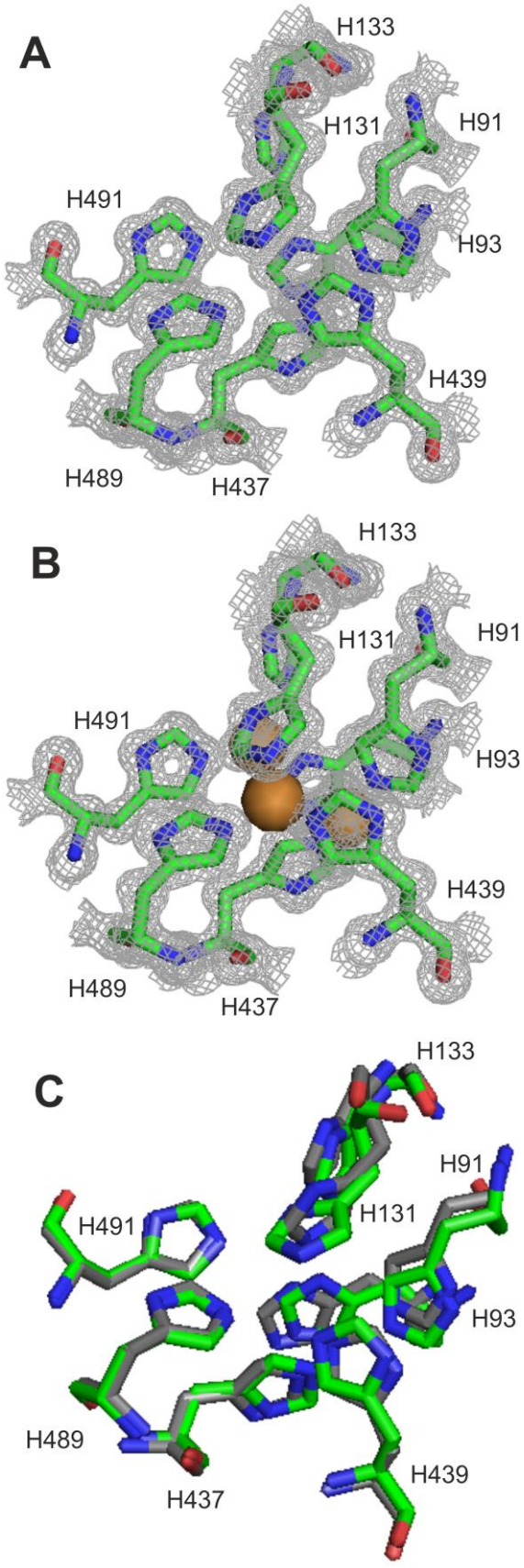
A
H133
H131
H91
H491
H93
H439
H489
H437
B
H133
H131
H91
H491
H93
H439
H489
H437
C
H133
H91
H491
H131
H93
H489
H439
H437

Figure 7.

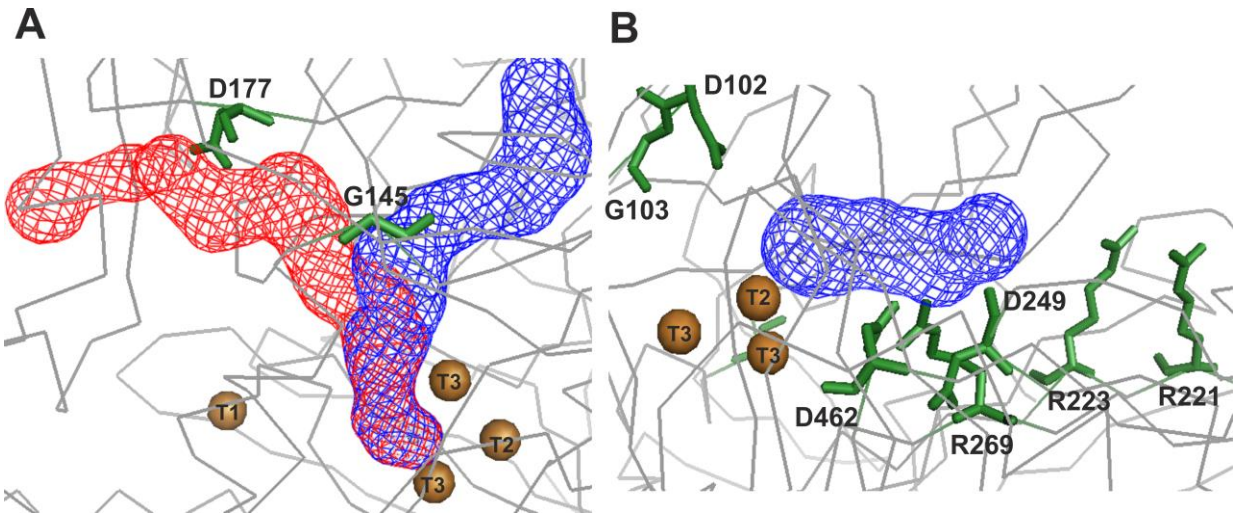

Figure 8.

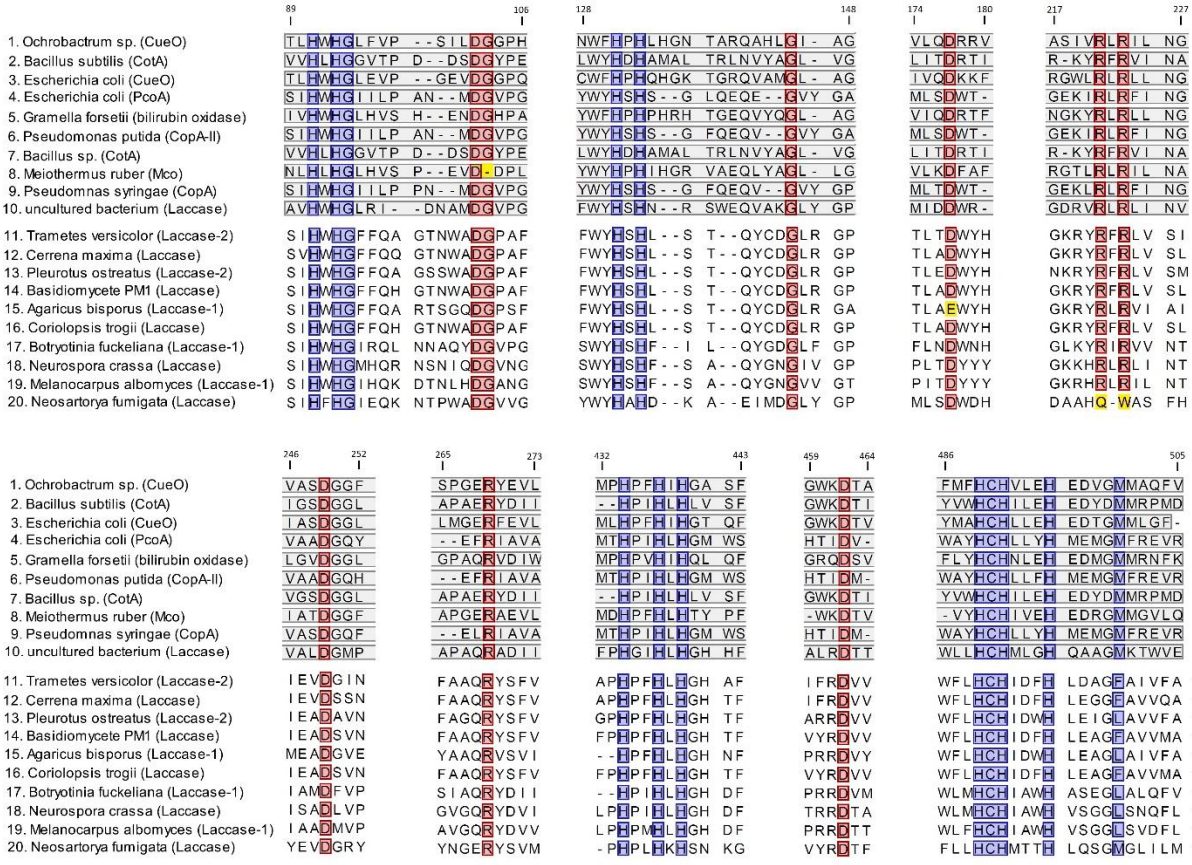

Figure 9.

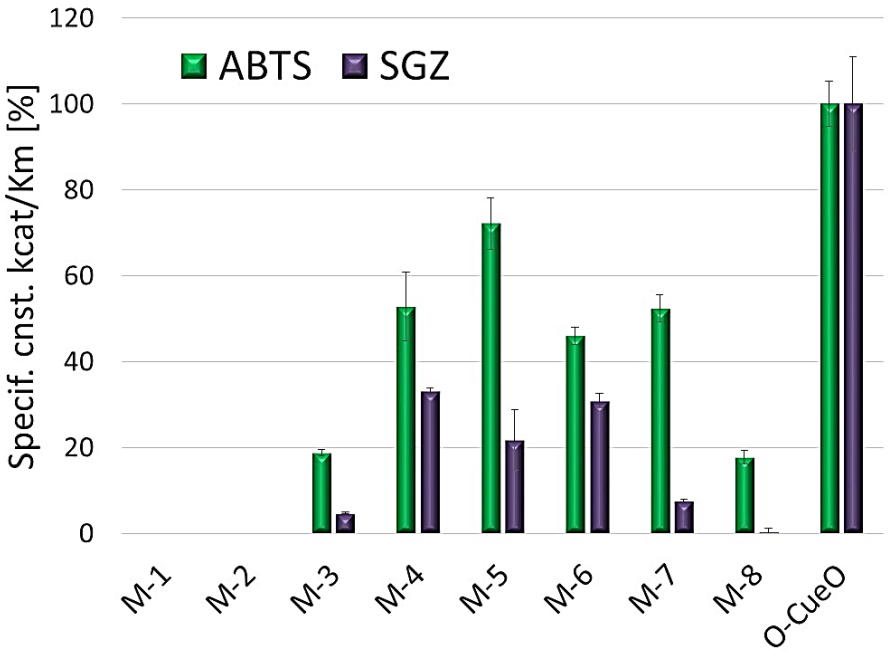
120
100
80
60
40
20
0
Specif. cnst. kcat/Km [%]
ABTS
SGZ
M-1
M-2
M-3
M-4
M-5
M-6
M-7
M-8
O-CueO